J Nanopart Res (2019) 21:118
https://doi.org/10.1007/s11051-019-4566-6

RESEARCH PAPER

Photothermal detection of a single gold nanoparticle in water suspension

Marcenilda Amorim Lima · Aristides Marcano Olaizola · Genaro López Gamboa · Maria Priscila Pessanha de Castro · Marcelo Silva Sthel

Received: 1 February 2019 / Accepted: 22 May 2019

Abstract We study the photothermal response of water solution of 10-, 50-, and 100-nm gold nanoparticles as a function of concentration under irradiation of a continuous wave 6-W 445-nm diode laser. The method allows determining concentrations as low 8×10^{-7} mg/ml, which corresponds to the detection of a single nanoparticle of 100- and 50-nm diameter or about 1000 nanoparticles of 10-nm diameter. The results demonstrate the application for the study of the optical response of a single nanoparticle in water suspension. We discuss the potential applications of the finding for detection of low concentration of biomolecules using a single nanoparticle.

Keywords Photothermal lens spectrometry · Detection of gold nanoparticles · Z-scan · Photothermal effects · Detection of biomolecules

M. A. Lima (✉) · M. P. P. de Castro · M. S. Sthel
Laboratory of Physics Sciences, North Fluminense State University, 28.013-602, Campos dos Goytacazes, Rio de Janeiro, Brazil
e-mail: marcenilda_stm@yahoo.com.br

A. M. Olaizola
Division of Physical and Computational Sciences, Delaware State University, 1200 North Dupont Highway, Dover, DE 19901, USA

G. L. Gamboa
Unidad Profesional Interdisciplinaria en Ingeniería y Tecnologías Avanzadas, Instituto Politécnico Nacional, 07340 Laguna Ticomán, Mexico

Introduction

Metal colloids and particles dissolved in water and other solvents have become a strong field of study for many researchers due to its potential applications in biophotonics and biomedicine (Pankhurst et al. 2003; Khlebtsov et al. 2006; Penn et al. 2003; Salata 2004; Sperling et al. 2008). Metallic nanoparticles present a phenomenon called surface plasmon resonance (SPR), in which free conduction electrons resonate collectively with the electromagnetic radiation, resulting in absorption peaks as well as dispersion (Jiang et al. 2013). Some studies have used nanoparticles with scientific and commercial interest for a wide range of biomedical applications (Lin et al. 2012), in vitro molecular diagnosis (Zhou et al. 2015), biologic and chemical detection sensors (Dykman and Khlebtsov 2012; Saha et al. 2012), cancer photothermal therapies (Abadeer and Murphy 2016; Huang and El-Sayed 2010; Kim and Lee 2017), and biological and pharmaceutical uses (Otsuka et al. 2012; Reddy et al. 2012; Zijlstra et al. 2012). Several authors have also used biosynthesized silver nanoparticles (Ag NPs) and alumina oxide nanoparticles added to diesel/biodiesel compound, aiming at analyzing its influences on combustion performance of diesel motor engine to determine gaseous emissions (Arockiasamy and Anand 2015; El-Seesy et al. 2018; Nireeksha et al. 2017). Gold, silver, and iron oxide nanoparticles generally show low toxicity, low cost, high radiation absorption, and biocompatibility with protein for applications in biomedical studies (Magro et al. 2018; Niska et al. 2018). In particular, gold

Published online: 03 June 2019

nanoparticles (Au NPs) have been the object of detailed analysis given their potential as a sensitizing agent in phototherapy thanks to their properties such as size, composition, high coefficients of absorbance, synthesis, and biocompatibility (Huang et al. 2007; Sperling et al. 2008). Au NPs act as photothermal agents for the cancer therapy treatment, because they present effective local heating after the excitation of the plasmon surface oscillations (Hwang et al. 2014).

Various studies in different research areas have been developed to determine the optical, electrical, and thermal properties of gold nanoparticles in aqueous solutions (Maceiczyk et al. 2017; Paulo et al. 2009; Yorulmaz et al. 2015). Consequently, there is a demand for sensitive techniques able to detect, identify, and quantify the level of these individual particles (Crut et al. 2014). Among these techniques, the laser dual-beam mode-mismatched photothermal lens (PTL) spectroscopy stands out thanks to its high sensitivity.

The PTL effect occurs due to the radiation absorbance by the sample, which, consequently, triggers local temperature changes and induces a variation in the refraction index, which results in a local thermal lens. The PTL effect accumulates due to a relatively slow process of thermal diffusion. Atoms absorb photons and convert their energy into heat for a period of 10^{-8} to 10^{-12} s. Thermal diffusion removes this heat, balancing back for about 10^{-2} s. Furthermore, one single atom can store in the solvent molecules the energy of 10^{6} to 10^{10} photons. For an individual NP, which contains from 10^{3} to 10^{6} atoms, this factor is substantially more significant. The NPs in water suspension release fast the absorbed energy toward the surrounding water molecules where heat accumulates thanks to the slow thermal diffusion of the water solvent.

Shahriari et al. (2016) used the PTL technique to investigate the thermal diffusivity by using polyvinylpyrrolidone solution samples with gold nanoparticles for different concentration rates. Eastman et al. (2004) and Paulo et al. (2009) studied heat transport through diluted suspensions of solid particles given the variation of thermal conductivity. Various studies have been developed by using PTL techniques to measure optical absorbance and colloid characterization with metal nanoparticles (Bialkowski and Mandelis 1996; Brusnichkin et al. 2007; Hleb and Lapotko 2008).

Marcano et al. (2001) proposed an optimized configuration of the mode-mismatched PTL method, which uses a collimated probe beam and a focused pump beam. The experiment allows detection of absorption as low as 10^{-8} cm^{-1} for liquids (Marcano et al. 2002, 2003). Brusnichkin et al. (2007) studied the detection of Au NPs with a photothermal lens technique. Hlaing et al. (2016) used the optimized mode-mismatched PTL technique to determine the absorption and scattering of light by silver nanoparticles. In the present work, we use an optimized pump-probe mode-mismatched PTL spectrometer aimed at detection of individual NPs in suspension. We demonstrate detection of a single NP of *50-* and *100-nm* diameter dispersed in water using a *6-W 445-nm* diode laser as a pump light source. The technique allows determination of the absorption cross-section of a single individual NP in interaction with the solvent molecules. We also report the detection in a water suspension of record low numbers of NPs of smaller diameter. The finding has potential applications to develop a highly sensitive method of detection of biomolecules conjugated with a single Au NP. The technique allows an intrinsically non-destructive analysis of microvolumes of the sample.

Theoretical considerations

Absorption measurement by using photothermal lens technique

In an optimized mode-mismatched PTL experiment, a lens focuses the pump laser onto the sample generating a rise in local temperature and variation in refraction index, yielding the PTL. Figure 1 presents an optimized mode-mismatched photothermal lens set-up. We consider that the pump and the probe radiations are Gaussian with Raleigh ranges z_{oe} and z_{op}, waist positions z_e and z_p, respectively. The probe beam is collimated, resulting in a large Rayleigh range ($z_{op} \gg z_{oe}$). The configuration optimizes the PTL experiment by providing the maximal sensitivity and simplifying the alignment procedure, the data interpretation, and the spectrophotometer calibration.

The PTL triggers changes in the wavefront of the probe beam. We define the PTL signal as the relative change of the probe transmittance through a small slit located at the far field. This way we account for the magnitude on distortions of the probe beam diffraction profile.

We use the model developed by Shen et al. (1992) based on the Fresnel's diffraction approximation which

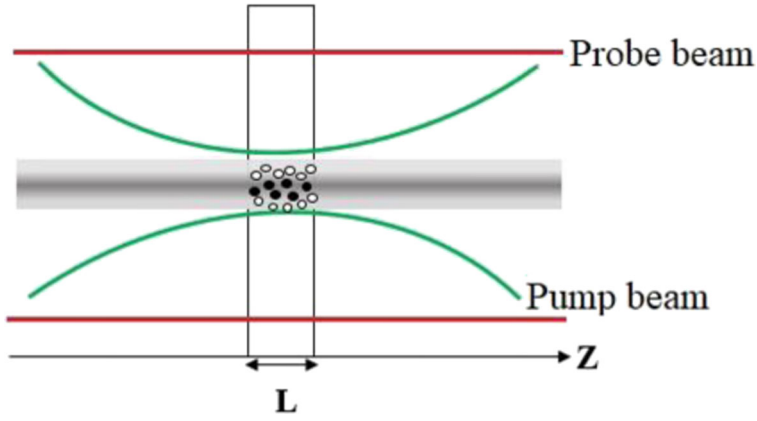

Fig. 1 Diagram of optimized mode-mismatched photothermal lens technique with Au NPs colloids

presents a description of a mode-mismatched experiment (Marcano et al. 2014; Shen et al. 1995; Shen et al. 1994). The model takes into account that the PTL signal phase modifies the probe beam wavefront, inducing variations in its diffraction pattern at the far field. We use the thin-lens approximation given the fact that the breadth of radiation beams does not vary significantly within the cuvette's width. We also consider the probe and pump beams to be Gaussian (Shen et al. 1994; Whinnery 1974; Marcano et al. 2002). The pump and probe beam have waist positions at z_e and z_p and Raleigh ranges z_{oe} and z_{op}, respectively. The sample is at position z. We scan the sample around the focal point of the pump field to generate the Z-scan. The pump and probe beam radii are, respectively

$$\omega_e(z) = \omega_{oe}\sqrt{1 + \frac{(z-z_e)^2}{{z_{oe}}^2}} \tag{1}$$

$$\omega_p(z) = \omega_{op}\sqrt{1 + \frac{(z-z_p)^2}{{z_{op}}^2}} \tag{2}$$

where $\omega_{oe} = \sqrt{\lambda_e z_{oe}/\pi}$ is the pump beam waist radius and λ_e is the pump beam wavelength, $\omega_{op} = \sqrt{\lambda_p z_{op}/\pi}$ is the probe beam waist radius, and λ_p is the probe beam wavelength. The volume defined by the pump beam within the sample can be calculated using Eq. (1) and performing the integration over the pathlength L of the cuvette. Considering $z_e = 0$, we obtain

$$\nu_o = L{\cdot}z_{oe}{\cdot}\lambda_e{\cdot}\left(1 + \frac{L^2}{3z_{oe}^2}\right) \tag{3}$$

The radiation absorption inside the sample generates a temperature change, which is a function of the sample position (z), the transversal coordinate (r), and time (t). The resolution of the Laplace's equation on heat diffusion provides the solution as (Shen et al. 1994; Whinnery 1974)

$$\Delta \mathrm{T}(\mathrm{z},\mathrm{t},\mathrm{r}) = -\frac{\alpha P_e}{4\pi k}\int_1^{1/(1+2\mathrm{t}/\mathrm{t_c}(\mathrm{z}))}\frac{\exp\left(-2xr^2/\omega_e(z)^2\right)}{x}\,dx \tag{4}$$

where $t_c(z) = \omega_e(z)^2/4D$ is the thermal lens build-up time, $D = k/\rho C_p$ is the thermal diffusivity coefficient, ρ is the sample's density, C_p is the specific heat, κ is the thermal conductivity, and P_e is the pump beam power. The variations caused in the refraction index come from the rise in the sample's temperature, which produces changes in the wavefront of the propagation beam. The thermal distribution generates a variation in probe beam phase, calculated in the thin lens approximation as (Marcano et al. 2002):

$$\Phi(\mathrm{z},\mathrm{t},\mathrm{r}) = \Phi_0\int_1^{1/(1+2\mathrm{t}/\mathrm{t_c}(\mathrm{z}))}\frac{1-\exp(-2xm(z)r)}{2x}\,dx \tag{5}$$

where the phase amplitude is $\Phi_0 = \alpha P_e L_{eff}(dn/dT)/(k\lambda_p)$, α is the sample's optical absorption coefficient, $L_{eff} = [1 - \exp(-\alpha L)]/\alpha$ corresponds to the sample's effective width, dn/dT is the refraction index variation with temperature, and $m(z) = \omega_p(z)^2/\omega_e(z)^2$ is the mode-matching parameter.

The phase variation $\Phi\ (z,\ t,\ r)$ impacts the probe beam propagation. Behind the sample's cuvette, the probe beam propagates until the slit position. The Fresnel diffraction approximation provides the beam's field at the detection plane (Shen et al. 1995; Marcano et al. 2002). This approximation allows the calculation of the magnitude of the

probe beam field $E(z,t)$ at the center of the detector as (Shen et al. 1994; Shen et al. 1992).

$$\mathrm{E}(\mathrm{z},\mathrm{t}) = \int_0^\infty \exp[-(1+iV(z))r - i\Phi(z,t,r)]dr \quad (6)$$

$$\mathrm{E}_0(\mathrm{z},\mathrm{t}) = \int_0^\infty \exp[-(1+iV(z))r]dr \quad (7)$$

where E_0 is the probe field's magnitude in the absence of the pump field, $i = \sqrt{-1}$,

$V(z) = \frac{z-z_p}{z_{op}} + \left(\frac{z_{op}}{d-z}\right)\left[1 + \frac{(z-z_b)^2}{z_{op}{}^2}\right]$ is the Fresnel diffraction parameter, and d is the position of the detection plane.

We define the PTL signal $S(z,t)$ as

$$\mathrm{S}(\mathrm{z},\mathrm{t}) = \frac{(|E(z,t)|)^2 - (|E_0(z,t)|)^2}{(|E_0(z,t)|)^2} \quad (8)$$

Materials and methods

Determination of the number of Au NPs particles

We study spherical Au NPs of different diameters: *10 nm*, *50 nm*, and *100 nm*. NanoComposix provided the original samples at a standard concentration of *0.05 mg/ml* and *99.99%* purity. Column 1 of Table 1 shows the diameter and their standard deviation as described by the provider. We estimate the mass of one single NP of a given dimension considering the particle a perfect sphere (see column 2 in Table 1). Column 3 of Table 1 shows the estimated values for the cross-section of absorption of a single nanoparticle. For this estimation, we use the Mie calculator provided at the NanoComposix website (https://nanocomposix.com/pages/mie-theory-calculator). We use the absorption cross-section values to estimate the absorption coefficient due to the presence of one single NP within the volume illuminated by the pump light (v_o) using the equation

$$\alpha = \sigma / v_o \quad (9)$$

where σ is the absorption cross-section. For calculation of v_o, we consider a 0.1-cm pathlength and a pump beam Rayleigh range of $z_{oe} = 0.3$ *cm*. These parameters are close to the conditions of the experiment discussed below. The absorption coefficient for pure water at *445 nm* is $5\ 10^{-5}\ cm^{-1}$ (Cruz et al. 2009). The effective absorption of one single Au NP of *10 nm* is well below this value. However, the absorption for *50* and *100 nm* is comparable to water absorption. Thus, it becomes feasible to detect a single nanoparticle of diameter larger than *50 nm*.

We reduce the sample concentration by adding distilled water to the original samples using a precision pipette. We use eq. (3) to estimate the volume v_o, as seen in Fig. 1. Hence, we determine the mass of the Au NPs (Δm_{AU}) contained in this volume. Thus, the number of nanoparticles detected is

$$\mathrm{N} = \frac{\Delta m_{AU}}{m_{AU}} \quad (10)$$

Table 1 Characteristics of spherical gold nanoparticles of different diameters

Diameter (nm)	Mass of a single nanoparticle (mg)	Absorption cross-section at 445 nm (nm^2)	Absorption coefficient of a single NP (cm^{-1})
12 ± 1	(1.3 ± 0.4) 10^{-14}	40 ± 10	(2.9 ± 0.7) × 10^{-7}
52 ± 5	(1.4 ± 0.4) 10^{-12}	3500 ± 1000	(2.6 ± 0.9) × 10^{-5}
103 ± 10	(1.1 ± 0.3) 10^{-11}	16,500 ± 2500	(1.2 ± 0.2) × 10^{-4}

Detection of Au NPs in aqueous solutions

We prepare eight solution samples in different culture tubes. We add *0.5 ml* of deionized distilled water, to *0.5 ml* of the sample with an initial concentration of *0.05 mg/ml* of Au NPs. Following this step, *0.5 ml* from this solution was taken and added to the second sample, thus reducing its initial concentration rates in half. After that, we perform the same procedure repeatedly along with the next samples aiming at obtaining the lowest nanoparticle concentration levels in each test tube. We conducted measurements using *0.1-cm*, *1-cm*, and *5-cm* wide quartz cuvettes. Figure 2 shows the optimized photothermal lens experimental apparatus used for obtaining the PTL signal, which is similar to the one developed by Marcano et al. (2014). This device consists of a diode laser modulated at *1 Hz* using a signal generator (GwInstek, GFG-3015). At this low frequency, the signal reaches its stationary value. The beam splitter (B_1) redirects a share of excitation radiation

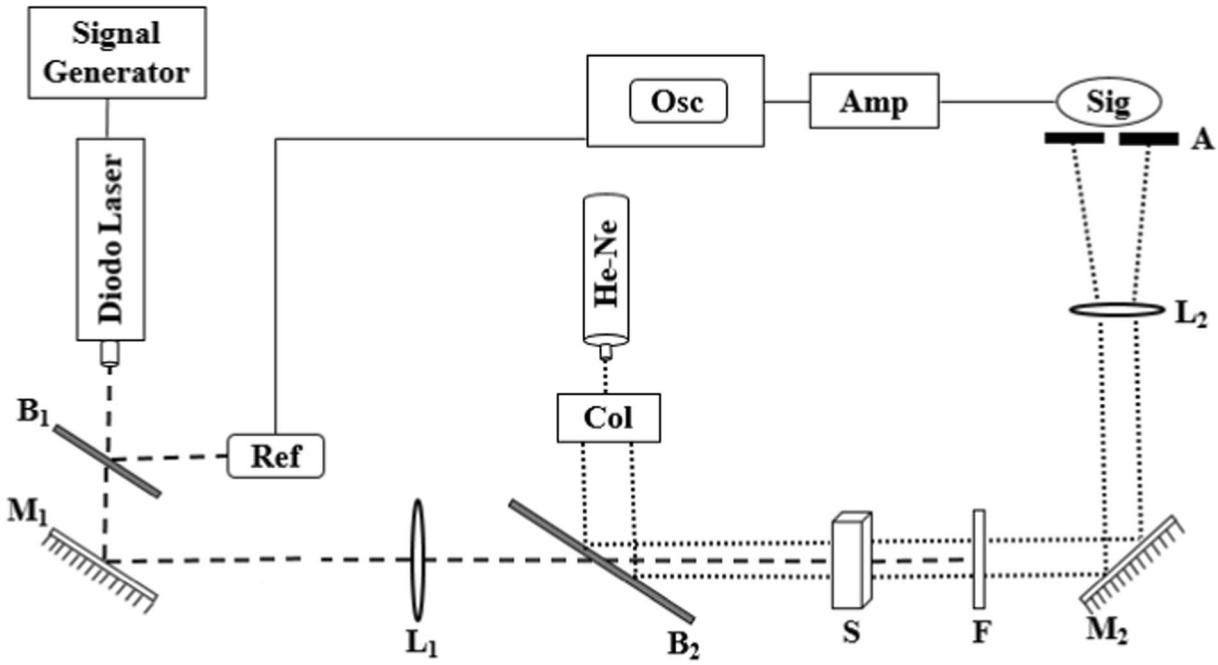

Fig. 2 Experimental configuration of high-sensitivity optimized mode-mismatched PTL spectrometer

towards the reference signal detector (Ref), which is connected to the digital oscilloscope (OSC) also used for the acquisition of the PTL signal. The mirror M_1 redirects the pump beam towards the sample, and a *15-cm* focal-length lens (L_1) focuses the light onto it. Behind the sample, we use an interference filter F to block the pump beam. A continuous wave CW of *1-mW* He-Ne laser at *632 nm* generates the probe beam. A telescope (Col) collimates this light resulting in a parallel beam of *3 mm* diameter. Using a beam splitter (B_2), we redirect the probe beam toward the sample collinearly with the pump beam. The PTL distorts the probe beam wavefront. Behind the sample, a mirror (M_2) sends the probe beam to a small slit (A) centered at the probe beam axis. A defocusing lens (L_2) defocuses this light making the effective radius of the aperture negligible. Behind the aperture, the probe light reaches the diode photodetector (Sig) (Thorlabs, DET 110) which measures the probe beam transmission yielding the PTL signal. A current preamplifier (Stanford Research Systems SR 570) amplifies the signal before sending it to a digital oscilloscope (Tektronix TDS3052) for processing.

The set-up allows performing Z-scan experiments by scanning the sample around the waist of the pump field. In the mode-mismatched configuration, the Z-scan curve is single peaked with a maximum at the focal point of the pump beam. The Z-scan experiments determine the position of the maximal PTL signal. By fitting the Z-scan results with the theoretical model described above, we obtain the value of the PTL phase shift amplitude $_o$, and the Rayleigh range z_e of the pump beam. We estimate the absorption values using the phase shift values. The Rayleigh range value yields the volume v_o (see Eq. 3).

Results and analysis

Z-scan on Au NPs samples

Figure 3a shows results obtained for Z-scan signals for each Au NPs colloid by using the procedure described by Hlaing et al. (2016). In this figure, one can observe the PTL signal regarding the sample position (Z-scan) of Au NPs with *10-nm*, *50-nm*, and *100-nm* diameters contained in a *1-cm* wide cuvette. We use *10 mW* of *532-nm* radiation from a DPSS laser. The signal generator modulates this light at *1 Hz*. The Z-scan experiment provides the position where the sample achieves its maximum absorbance, depicting one single peak at the pump beam waist whose magnitude is proportional to the sample absorption. The solid lines correspond to theoretical fittings of the experimental Z-scan curves

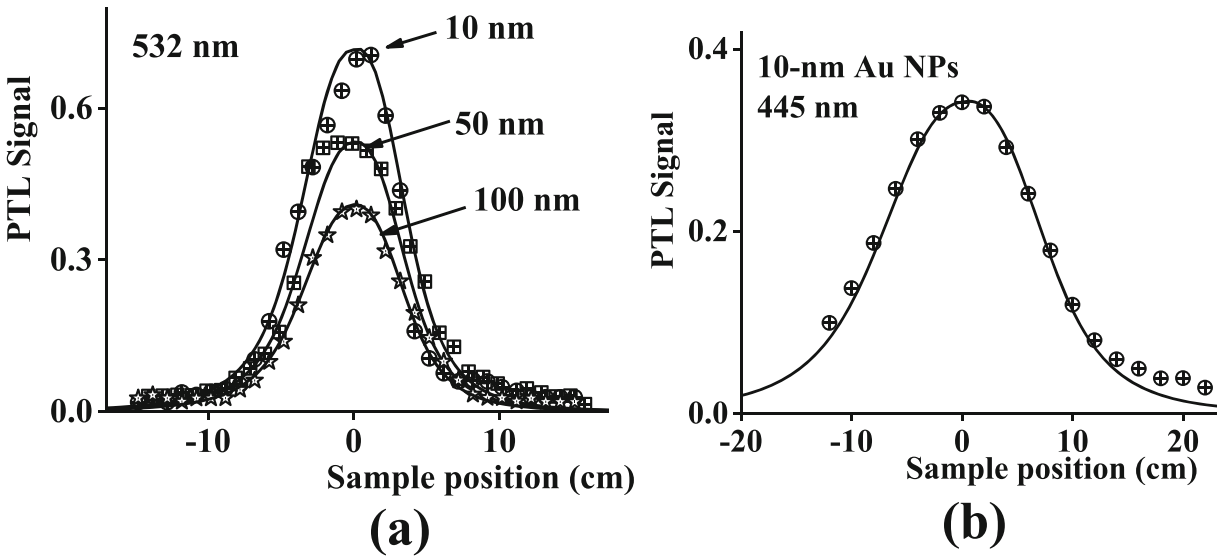

Fig. 3 **a** PTL Z-scan of the *10-nm*, *50-nm*, and *100-nm* original solutions measured using *10 mW* from a *532-nm* DPSS laser. The solid lines are theoretical fittings calculated using eqs. 6 through 9 and the parameters $\lambda_p = 632\ nm$, $\lambda_e = 532\ nm$, $z_e = 0.16\ cm$, $z_p = 1000\ cm$, $D = 1.4\ 10^{-3}\ cm^2\ s^{-1}$, $_o = -0.27, -0.204,$ *and* -0.16 for the *10-nm*, *50-nm*, and *100-nm* samples, respectively. **b** PTL Z-scan of the *10-nm* sample measured using *36 mW* from a *445-nm* diode laser. The solid line is a theoretical fitting calculated using eqs. 6 through 9 and the parameters $\lambda_p = 632\ nm$, $\lambda_e = 445\ nm$, $z_e = 0.3\ cm$, $z_p = 1000\ cm$, $D = 1.4\ 10^{-3}\ cm^2\ s^{-1}$, $_o = -0.18$

calculated using eqs. 6 through 9. In this calculation, we use the parameters: $\lambda_p = 632\ nm$, $\lambda_e = 532\ nm$, $z_{op} = 1000\ cm$, $z_{oe} = 0.16\ cm$, $t = 0.5\ s$, $z_e = z_p = 0$, $d = 50\ cm$, and $D = 1.4\ 10^{-3}\ cm^2\ s^{-1}$, which corresponds to the water diffusivity value. The fitting gives the values of the induced phase shift $_o$: -0.27, -0.2, and -0.16 for the *10-*, *50-*, and *100-nm* diameter Au NPs, respectively. Considering the values for water $\kappa = 6\ 10^{-3}\ Wcm^{-1}\ °K^{-1}$, $dn/dt = 1.1\ 10^{-4}\ °K^{-1}$ and the length of the cuvette $L = 1\ cm$, we estimate absorptions values of *0.093*, *0.068*, and *0.055* cm^{-1} for *10-*, *50-*, and *100-nm* diameter Au NP samples, respectively. The values

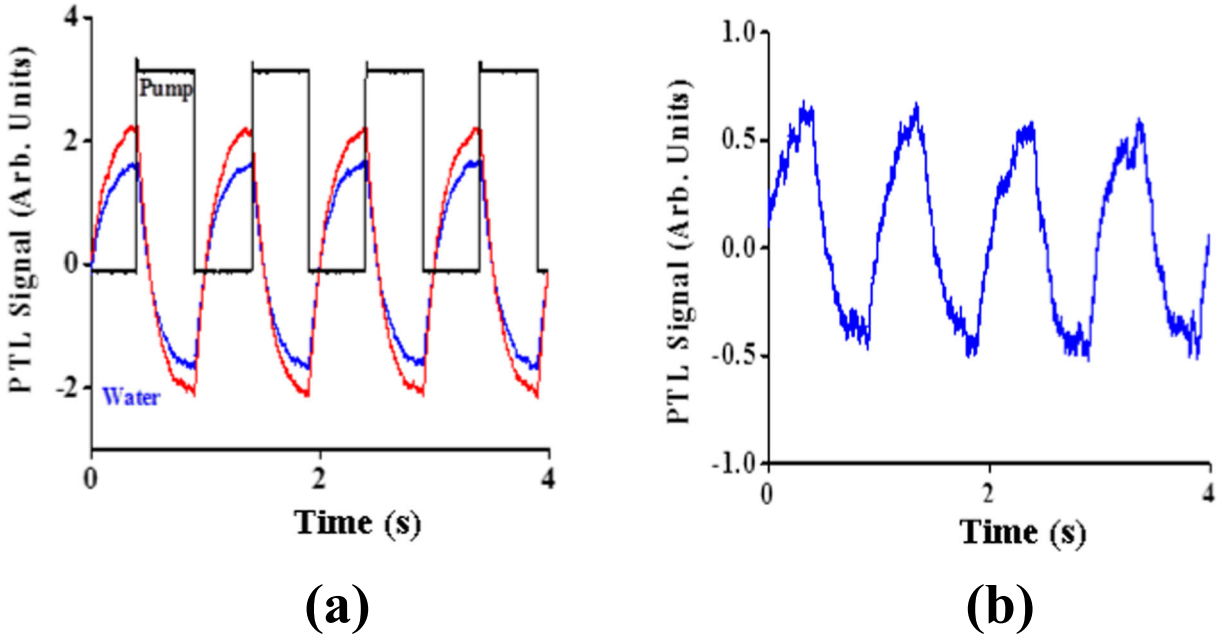

Fig. 4 **a** PTL signal versus time for *1-μl* of *10-nm* 6.2×10^{-3} *mg/ml* Au NPs colloid. **b** Same signal after subtraction of water contribution

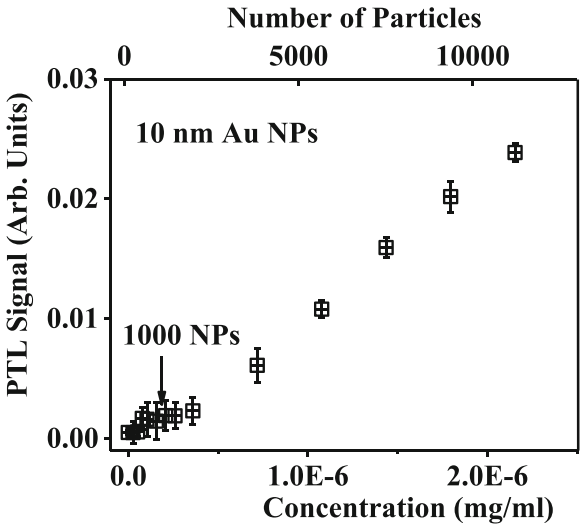

Fig. 5 PTL signal versus concentration and number of NPs for the *10-nm* diameter Au NPs sample using *220 mW* of *445 nm* radiation and a 1-cm pathlength cuvette. The zero point represents the PTL signal for pure water

agree well with the prediction for the absorption of the Mie model. The reduction of the absorption for larger NPs is due to the presence of scattering (Hlaing et al. 2016). For *100-nm* Au NPs, more than *60%* of the incoming light is scattered reducing the power available for heating. The scattering is negligible for 10-nm Au NPs. Figure 3b shows similar results obtained for *10-nm* Au NPs using *36 mW* of *445-nm* blue diode laser radiation as pump light. The solid line corresponds to a theoretical fitting using eqs. 6 through 9 and parameters $\lambda_p = 632\ nm$, $\lambda_e = 445\ nm$, $z_p = 1000\ cm$, $z_e = 0.3\ cm$, $d = 100\ cm$, $_o = -0.185$, $D = 1.4\ 10^{-3}\ cm^2\ s^{-1}$, and $t = 0.5\ s$. For this excitation wavelength, we estimate an absorption of $0.018\ cm^{-1}$, which is smaller than the plasmonic near peak absorption at 532 nm. We compensate the smaller absorption by using larger power from the *445-nm* laser, so the magnitudes of the PTL signal are comparable to those obtained when using *10 mW* of *532-nm* pump light.

On the other hand, the background absorption of water at *445 nm* is much smaller than its value at *532 nm*. Thus, it is advantageous to use excitation in the blue region where water produces minimal losses. Below, we conduct the experiments using excitation at 445 nm reducing the background water contribution substantially.

Properties of the nanoparticle can be affected when using high energy light pulses. When irradiating with nanosecond high energy pulses with fluence levels above the NP damage threshold, NP melting and generation of microbubbles have been reported (Hleb and Lapotko 2008). When using CW excitation as in this work, the effective energy fluence is well below the damage threshold. The AU NPs release the absorbed

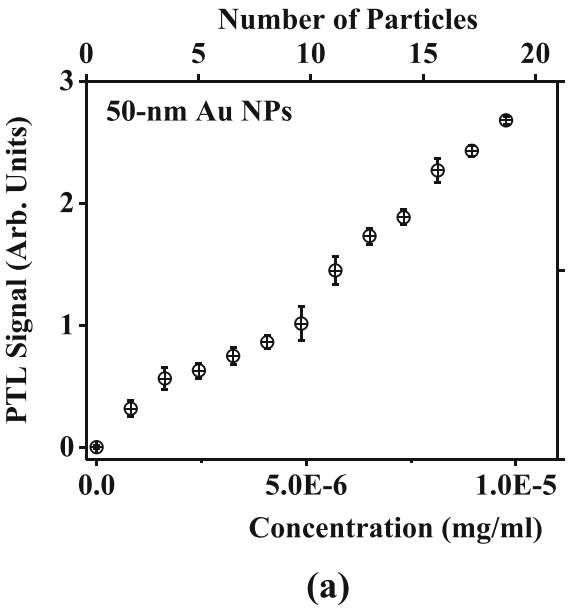

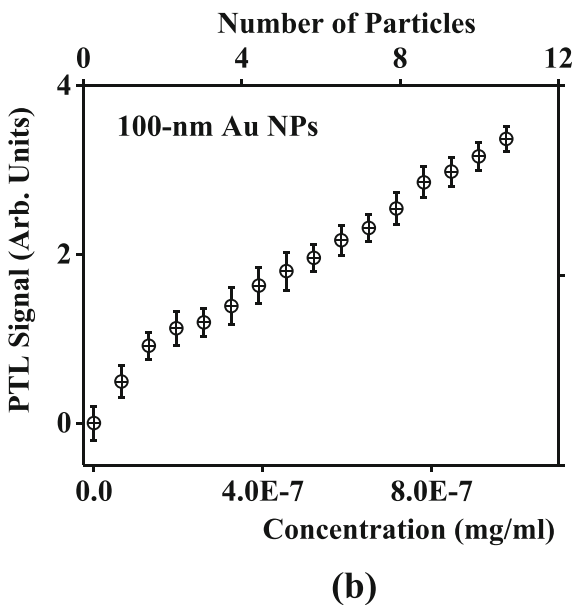

Fig. 6 **a** PTL signal versus concentration and number of particles for *50-nm* Au NPs solution using 1-mm pathlength cuvette. The zero point represents the PTL signal for pure water. **b** PTL signal versus concentration and number of NPs for *100-nm* Au NPs solutions using a *1-cm* pathlength cuvette

Table 2 Parameters of gold nanoparticle solutions for different diameters (optical parameters for 445 nm)

NP diameter (nm)	Concentration (mg/ml)	Cell width (cm)	NPs mass in 1 μl	NPs concentration (mg/ml)	v_o (cm^3)	NPs mass in v_o (mg)	Number of NPs detected
10	0.39×10^{-3}	1	0.39×10^{-6}	2.60×10^{-8}	7.046×10^{-5}	1.83×10^{-12}	130
10	0.78×10^{-3}	5	0.78×10^{-6}	7.80×10^{-8}	3.523×10^{-4}	3.01×10^{-12}	200
50	1.95×10^{-4}	0.1	1.95×10^{-7}	1.30×10^{-8}	7.046×10^{-5}	0.92×10^{-12}	1
50	9.76×10^{-5}	1	9.76×10^{-8}	3.25×10^{-8}	7.046×10^{-5}	2.29×10^{-12}	2
50	0.39×10^{-3}	0.1	0.39×10^{-6}	1.62×10^{-6}	1.172×10^{-6}	1.90×10^{-12}	1
100	0.78×10^{-3}	1	0.78×10^{-6}	2.60×10^{-7}	7.046×10^{-5}	1.83×10^{-11}	2
100	1.95×10^{-4}	1	1.95×10^{-7}	6.50×10^{-8}	7.046×10^{-5}	4.58×10^{-12}	1
100	9.76×10^{-5}	1	9.76×10^{-8}	3.25×10^{-8}	7.046×10^{-5}	2.29×10^{-12}	1

electromagnetic energy in a time scale of few picoseconds. The energy accumulates in the surrounding water molecules where local changes in the temperature are estimated as well below one degree thanks to the larger volume of the solvent involved, the limited amount of energy absorbed, and the thermal properties of water. We have established that the PTL response of the samples depends linearly on the power levels used in the experiments in agreement with the prediction that the photothermal properties of the samples are not affected.

Removing the water contribution

For small concentrations of NPs, the contribution from pure water becomes significant. However, we estimate the signal corresponding to the NPs by simple subtraction of the water contribution. Figure 4a shows the maximal PTL signal versus time for water and the 10-nm diameter Au NP sample at a concentration of 6.2×10^{-3} *mg/ml* generated by a *20-mW* (*445 nm*) pump beam. For comparison, we add the modulated at *1 Hz* pump beam time dependence. Despite the small concentration, the Au NP sample gives a measurable signal. Figure 4b shows the signal from the Au NPs after removing the water contribution by subtraction of both curves in Fig. 4a. From this plot, we estimate a signal-to-noise ratio of *20*.

Detecting a single Au NP

Figure 5 shows the maximal PTL signal versus the concentration rate for the *10-nm* diameter Au NPs sample generated by *220 mW* by using the *1-cm* pathlength cuvette after the cancelation of the water contribution. On the top scale, we show the corresponding number of nanoparticles. We estimate the volume defined by the pump beam within the sample (v_o) using Eq. 3 and the Rayleigh range value of the pump determined by the Z-scan experiment shown in Fig. 3b ($z_{oe} = 0.3$ *cm*).

We use a minimal concentration of $2.6\ 10^{-7}$ *mg/ml* which corresponds to having around *1000* NPs in the volume v_o. The number of particles corresponds well to the estimation of the absorption of a single NP absorption shown in Table 1.

Figure 6a shows the PTL signal as a function of concentration and number of particles (top scale) for the *50-nm* Au NPs sample. We use *280 mW* of the *445-nm* radiation and a *0.1-cm* pathlength quartz cuvette. To generate the data, we add 1 μl of a dilute solution of a concentration of $1.95\ 10^{-4}$ *mg/ml* to *0.24 ml* of water. The procedure enabled the detection of a single Au NP. Furthermore, the experiment showed two distinct behaviors in the curve. Initially, when adding *1 μl* of nanoparticle solution to the water, it was revealed a visible non-linear rise in concentration with PTL signal, which is possibly caused by the increase in NP concentration, by occurring density saturation in an aqueous environment. Right above 4.0×10^{-6} *mg/ml*, it is noted linearity, once the "thermal lens" is proportional to the NP concentration in the sample and the thermal-optical properties of the environment.

According to Shahriari et al. (2016), the increase in concentration and in gold nanoparticle size presented a non-linear growth in thermal diffusivity, due to the phenomena of phonon dispersion between liquid-particle interfaces. Moreover, when particle concentration rises, the optical absorption intensity becomes more significant, as well as the thermal diffusivity in an aqueous environment.

Figure 6b illustrates the results for the *100-nm* Au NP sample. We use *280 mW* of the *445-nm* radiation and *1-cm* pathlength cuvette, and an initial concentration of 1.95×10^{-4} mg/ml. The PTL signal raises as we add additional 1-μl drops of the solution. The non-linear behavior presents a smaller quantity of experimental points relative to the *50-nm* Au NPs case. The effect probably happens given the size proportions of the nanoparticle, which can better absorb or disperse radiation. The results confirm the detection of a single Au NP.

Table 2 displays the parameters of different PTL experiments using the pump beam at a wavelength of *445 nm*. The table provides the Au NPs diameters used, the initial concentration for each experiment, the cuvette width, the total volume of distilled deionized water used, the mass of NPs contained in *1 ml* of the original concentration, the excitation volume v_o, the mass of the NPs in the volume v_o, the amount of Au NPs mass in the volume v_o, and the number of NPs derived from the eq. 10. The sensitivity in optimized mode-mismatched thermal lens technique shows a distinct NPs AU dependence detected according to the pump beam's volume, which crosses through the sample. The *10-nm* diameter nanoparticles presented higher amounts of NP detected, due to its smaller diameter. For 50-nm and 100-nm diameter nanoparticles, we report the detection of one individual Au NP.

Conclusion

We confirm that the optimized mode-mismatched photothermal lens spectrometry can we detect up to a single Au NP of a diameter larger than *50 nm* in water suspension. We demonstrate this sensitivity by using several hundreds of mW of 445-nm diode laser radiation. At this wavelength, water exhibits minimal absorption. However, the experiments can be performed using the most common DPSS laser at *532 nm*, for which the light absorption by water is larger but still small enough to obtain a similar result. We calibrate the spectrometer by performing Z-scan experiments, which determine the magnitude of the absorption and the Rayleigh parameters of the beams.

Funding information The Brazilian agency CAPES financially supported the sandwich doctorate scholarship of the student M. Lima in the Delaware State University. A. Marcano was provided support from the US National Science Foundation (awards 1831332, 1744502, and 1719379), G. López was financially supported by the Mexican Agencies CONACYT and the CCA-IPN.

Compliance with ethical standards

Conflict of interest The authors declare that they have no conflict of interest.

References

Abadeer NS, Murphy CJ (2016) Recent progress in cancer thermal therapy using gold nanoparticles. J Phys Chem 120:4691–4716. https://doi.org/10.1021/acs.jpcc.5b11232

Arockiasamy P, Anand R (2015) Performance, combustion and emission characteristics of a DI diesel engine fuelled with nanoparticle blended Jatropha biodiesel. Period Polytech Mech Eng 59:88–93. https://doi.org/10.3311/PPme.7766

Bialkowski SE, Mandelis A (1996) Photothermal spectroscopy methods for chemical analysis. Phys Today 49:76–76. https://doi.org/10.1063/1.2807813

Brusnichkin AV, Nedosekin DA, Proskurnin MA, Zharov VP (2007) Photothermal lens detection of gold nanoparticles: theory and experiments. Appl Spectros 61:1191–1201. https://doi.org/10.1366/000370207782597175

Crut A, Maioli P, del Fatti N, Vallée F (2014) Optical absorption and scattering spectroscopies of single nano-objects. Chem Soc Rev 43:3921–3956. https://doi.org/10.1039/C3CS60367A

Cruz RA, Marcano A, Jacinto C, Catunda T (2009) Ultrasensitive thermal lens spectroscopy of water. Opt Lett 34:1882–1884. https://doi.org/10.1364/OL.34.001882

Dykman L, Khlebtsov N (2012) Gold nanoparticles in biomedical applications: recent advances and perspectives. Chem Soc Rev 41:2256–2282. https://doi.org/10.1039/C1CS15166E

Eastman JA, Phillpot SR, Choi SUS, Keblinski P (2004) Thermal transport in nanofluids. Annual Rev Mat Res 34:216–246. https://doi.org/10.1146/annurev.matsci.34.052803.090621

El-Seesy AI, Attia AMA, El-Batsh HM (2018) The effect of aluminum oxide nanoparticle addition with jojoba methyl ester-diesel fuel blend on a diesel engine performance, combustion and emission characteristics. Fuel 224:147–166. https://doi.org/10.1016/j.fuel.2018.03.076

Hlaing M, Gebear-Eigzabher B, Roa A, Marcano A, Radu D, Lai CY (2016) Absorption and scattering cross-section extinction values of silver nanoparticles. Opt Mat 58:439–444. https://doi.org/10.1016/j.optmat.2016.06.013

Hleb EY, Lapotko DO (2008) Photothermal properties of gold nanoparticles under exposure to high optical energies. Nanotechnology 19:355702. https://doi.org/10.1088/0957-4484/19/35/355702

Huang X, El-Sayed MA (2010) Gold nanoparticles: optical properties and implementation in cancer diagnosis and photothermal therapy. J Adv Res 1:13–28. https://doi.org/10.1016/j.jare.2010.02.002

Huang X, Jain PK, el-Sayed IH, el-Sayed MA (2007) Gold nanoparticles: interesting optical properties and recent

applications in cancer diagnostics and therapy. Nanomedicine 2:681–693. https://doi.org/10.2217/17435889.2.5.681

Hwang S, Nam J, Jung S, Song J, Doh H, Kim S (2014) Gold nanoparticle mediated photothermal therapy: current status and future perspectives. Nanomedicine 9:2003–2022. https://doi.org/10.2217/nnm.14.147

Jiang K, Smith DA, Pinchuk A (2013) Size-dependent photothermal conversion efficiencies of plasmonically heated gold nanoparticles. J Phys Chem C 117:27073–27080. https://doi.org/10.1021/jp409067h

Khlebtsov B, Zharov V, Melnikov A, Tuchin V, Khlebtsov N (2006) Optical amplification of photothermal therapy with gold nanoparticles and nanoclusters. Nanotechnology 17:5167–5179. https://doi.org/10.1088/0957-4484/17/20/022

Kim HS, Lee DY (2017) Photothermal therapy with gold nanoparticles as an anticancer medication. J Pharm Investig 47:19–26. https://doi.org/10.1007/s40005-016-0292-6

Lin M, Zhao Y, Wang SQ, Liu M, Duan ZF, Chen YM, Li F, Xu F, Lu TJ (2012) Recent advances in synthesis and surface modification of lanthanide-doped upconversion nanoparticles for biomedical applications. Biotechnol Adv 30:1551–1561. https://doi.org/10.1016/j.biotechadv.2012.04.009

Maceiczyk R, Shimizu H, Müller D, Kitamori T, deMello A (2017) A photothermal spectrometer for fast background-free detection of individual nanoparticles in flow. Anal Chem 89:1994–1999. https://doi.org/10.1021/acs.analchem.6b04540

Magro M, Baratella D, Bonaiuto E, de A. Roger J, Vianello F (2018) New perspectives on biomedical applications of iron oxide nanoparticles. Current Med Chem 25:540–555. https://doi.org/10.2174/0929867324666170616102922

Marcano A, Loper C, Melikechi N (2001) High sensitivity absorption measurment in water and glass samples using a mode-mismtached pump-probe thermal lens method. Appl Phys 78:3415–3417. https://doi.org/10.1063/1.1375835

Marcano A, Loper C, Melikechi N (2002) Pump-probe mode-mismatched thermal-lens Z-scan. J Opt Soc Am B 19:119–124. https://doi.org/10.1364/JOSAB.19.000119

Marcano A et al (2003) Mode-mismatched thermal lens experiment in the pulse regime. J Opt A Pure Appl Opt 5:S256–S261. https://doi.org/10.1088/1464-4258/5/5/375

Marcano A, Alvarado S, Meng J, Caballero D, Moares EM, Edziah R (2014) White light photothermal lens spectrophotometer for the determination of absorption in scattering samples. Appl Spectros 68:680–685. https://doi.org/10.1366/13-07385

Nireeksha K et al (2017) Ecofriendly synthesis of silver nanoparticles using oil seed cake and its application in biodiesel for performance evaluation of 4 stroke diesel engine. Energy Power 7:75–80. https://doi.org/10.5923/j.ep.20170703.04

Niska K et al (2018) Metal nanoparticles in dermatology and cosmetology:interactions with human skin cells. Chem Biol Interact 295:38–51. https://doi.org/10.1016/j.cbi.2017.06.018

Otsuka H, Nagasaki Y, Kataoka K (2012) PEGylated nanoparticles for biological and pharmaceutical applications. Adv Drug Deliv Rev 55:403–419. https://doi.org/10.1016/S0169-409X(02)00226-0

Pankhurst QA, Connolly J, Jones SK, Dobson J (2003) Applications of magnetic nanoparticles in biomedicine. J Phys D Appl Phys 36:R167–R181. https://doi.org/10.1088/0022-3727/36/13/201

Paulo PMR, Gaiduk A, Kulzer F, Krens SFG, Spaink HP, Schmidt T, Orrit M (2009) Photothermal correlation spectroscopy of gold nanoparticles in solution. J Phys Chem 113:11451–11457. https://doi.org/10.1021/jp806875s

Penn SG, He L, Natan MJ (2003) Nanoparticles for bioanalysis. Curr Opin Chem Biol 7:609–615. https://doi.org/10.1016/j.cbpa.2003.08.013

Reddy LH, Arias JL, Nicolas J, Couvreur P (2012) Magnetic nanoparticles: design and characterization, toxicity and biocompatibility pharmaceutical and biomedical applications. Chem Rev 112:5818–5878. https://doi.org/10.1021/cr300068p

Saha K, Agasti SS, Kim C, Li X, Rotello VM (2012) Gold nanoparticles in chemical and biological sensing. Chem Rev 112:2739–2779. https://doi.org/10.1021/cr2001178

Salata OV (2004) Applications of nanoparticles in biology and medicine. J Nanobiotechnol 2:1–6. https://doi.org/10.1186/1477-3155-2-3

Shahriari E, Moradi M, Raeisi M (2016) An experimental study of thermal diffusivity of au nanoparticles: effects of concentration particles size. J Theor Appl Phys 10:259–263. https://doi.org/10.1007/s40094-016-0224-x

Shen J, Lowe RD, Snook RD (1992) A model for cw laser induced mode-mismatched dual-beam thermal lens spectrometry. Chem Phys 165:385–396. https://doi.org/10.1016/0301-0104(92)87053-C

Shen J, Baesso ML, Snook RD (1994) Three-dimensional model for cw laser-induced mode-mismtached dual-beam thermal lens spectrometry and time-resolved measurement of thin-film samples. J Appl Phys 75:3738–3748. https://doi.org/10.1063/1.356046

Shen J, Soroka AJ, Snook RD (1995) A model for cw laser induced mode-mismtached dual-beam thermal lens spectrometry based on probe beam profile image detection. J Appl Phys 78:700–708. https://doi.org/10.1063/1.360329

Sperling RA, Rivera Gil P, Zhang F, Zanella M, Parak WJ (2008) Biological applications of gold nanoparticles. Chem Soc Rev 37:1896–1908. https://doi.org/10.1039/B712170A

Whinnery JR (1974) Laser measurement of optical absorption in liquids. Acc Chem Res 7:225–231. https://doi.org/10.1021/ar50079a003

Yorulmaz M, Nizzero S, Hoggard A, Wang LY, Cai YY, Su MN, Chang WS, Link S (2015) Single-particle absorption spectroscopy by photohtermal contract. Nano Lett 15:3041–3047. https://doi.org/10.1021/nl504992h

Zhou W, Gao X, Liu D, Chen X (2015) Gold nanoparticles for in viro diagnostics. Chem Rev 115:10575–10636. https://doi.org/10.1021/acs.chemrev.5b00100

Zijlstra P, Paulo PMR, Orrit (2012) Optical detection of single non-absorbing molecules using the surface plasmon resonance of a gold nanorod. Nat Nanotechnol 7:379–382. https://doi.org/10.1038/nnano.2012.51